Dalton Transactions

Chiral weak ferromagnets formed in one-dimensional organic-inorganic hybrid manganese chloride hydrates

Journal:	*Dalton Transactions*
Manuscript ID	DT-ART-09-2022-002928.R1
Article Type:	Paper
Date Submitted by the Author:	30-Sep-2022
Complete List of Authors:	Taniguchi, Kouji; Tokyo Institute of Technology School of Science, Department of Chemistry; Japan Science and Technology Agency, PRESTO Huang, Po-Jung; Northwestern University, Materials Science and Engineering Kimura, Shojiro; Tohoku University, Institute for Materials Research Miyasaka, Hitoshi; Tohoku University, Institute for Materials Research; Tohoku University, Department of Chemistry, Graduate School of Science

ARTICLE

Chiral weak ferromagnets formed in one-dimensional organic-inorganic hybrid manganese chloride hydrates

Received 00th January 20xx,
Accepted 00th January 20xx

DOI: 10.1039/x0xx00000x

Kouji Taniguchi,*[a] Po-Jung Huang, [b] Shojiro Kimura [c] and Hitoshi Miyasaka [c]

Chiral weak ferromagnets were developed in organic-inorganic hybrid systems of one-dimensional manganese(II) chloride hydrate with chiral organic cations of (*S*)- and (*R*)-*β*-methylphenethylammonium (= (*S*)- and (*R*)-MPA$^+$), [(*S*)/(*R*)-MPA]$_2$[MnCl$_4$(H$_2$O)]. The weak ferromagnetic phase found in temperatures below 3.2 K could be attributed to a spin canting antiferromagnetic state induced by Dzyaloshinskii–Moriya interaction owing to spatial inversion symmetry breaking in the chirality introduced systems. This is the first chiral weak ferromagnet found in a spin chain of deformed perovskite derivatives with corner-sharing structure of transition metal halide hydrates.

Introduction

Chiral magnetic materials have been intensively investigated as promising platforms for producing novel quantum phenomena, such as magneto-chiral dichroism,[1-7] nonreciprocal electrical conduction,[8-11] and magnetic skyrmion.[12-14] In particular, the chiral magnets with spontaneous magnetization have been attracted much attention, because simultaneous breaking of spatial inversion- and time reversal-symmetries in such systems gave a good opportunity to allow coupling magnetism with dielectric property, e.g., magnetoelectric (ME) effect, in a material.[14,15]

For the purpose of developing new chiral magnetic materials, a class of low-dimensional organic-inorganic hybrid metal-halide perovskites (OIHPs) is one of the promising candidate materials. In two-dimensional (2D) OIHPs with anionic metal-halide perovskite layers (i.e., anionic inorganic layers), the chirality can be introduced by coulombically assembling chiral organic cations (i.e., cationic organic layers) that could be located between the anionic inorganic layers.[15-20] In fact, the chiral ferromagnets have successfully been obtained in 2D-OIHPs using copper(II) chloride based on this approach, and they revealed the optical ME effect.[15,21] On the other hand, chiral systems of one-dimensional (1D) OIHPs and their relevant deformed perovskite derivatives (totally, hereafter denoted as 1D-OIHPs) have also been synthesized so far, in which specific optical properties such as non-linear optical effect,[22] circular polarized light sensitivity,[23,24] and photovoltaic effect[25] were actually characterized. However, they were all constructed with non-magnetic lead halides, and therefore, arguments concerning chiral magnetism, which are anticipated in the family of chiral 1D-OIHPs comprising magnetic transition metal ions, have never been done.

Here, we report a chiral enantiomer set of 1D-OIHPs comprising manganese(II) chloride hydrate, [(*S*)/(*R*)-MPA]$_2$[MnCl$_4$(H$_2$O)] (***S*-1/*R*-1**), where (*S*)- and (*R*)-MPA$^+$ are (*S*)- and (*R*)-*β*-methylphenethylammonium cations, respectively.

A number of 1D chain complexes composed of a manganese halides core as in ***S*-1/*R*-1** have been comprehensively studied due to their intrachain antiferromagnetic coupling, the possible red-light emission, and ferroelectricity.[26-30] From the structural point of view, these complexes can be categorized into three groups by the number of bridging halide ion between each two Mn(II) ions. Based on the literatures, the structure of utilized cations strongly affects the intrachain bridging mode: 1) Simple cations such as Rb$^+$,[31] [NH$_2$(CH$_3$)$_2$]$^+$,[32] and CH$_3$NH$_3^+$ ions[33] and aromatic cations with a linear functional group over three non-hydrogen atoms such as (R/S)-MPA$^+$ in this work and PhCH$_2$NH$_2$CH$_3^+$ ion[34] result in singly-bridged/corner-shared mode with a [MnCl$_4$(H$_2$O)]$^{2-}$ or a [MnCl$_3$(H$_2$O)$_2$]$^-$ core. 2) Heterocyclic cations such as 2-aminoprydine derivatives[35,36] and imidazole derivatives[27,37] lead to doubly-bridged/edge-shared mode with a [MnCl$_3$(H$_2$O)]$^-$ core. 3) Long chain or large planar cations such as tetrathiafulvalene derivatives[38,39] and tert-butylprolinate[40] give triply-bridged/face-shared mode with a [MnCl^3]$^-$ core. Based on the limited numbers of literatures, which includes magnetic characterization for these 1D Mn chains, antiferromagnetic interactions exist regardless of the type of chloride bridging mode.[26,35,38,39] The chiral compounds among these complexes were reported to show circularly polarized luminescence and ferroelectricity, but no magnetic properties were studied.[40,41] Besides the structures with a [MnCl$_2$] core, 1D chains with a more complicate repeating unit can be obtained by utilizing ligands with coordinating ability.[42,43]

[a] *Department of Chemistry, School of Science, Tokyo Institute of Technology, 2-12-1 Ookayama, Tokyo, 152-8551, Japan.*
[b] *PRESTO, Japan Science and Technology Agency (JST), 5-3 Yonbancho, Chiyoda-ku, Tokyo 102-8666, Japan.*
[c] *Institute for Materials Research, Tohoku University, 2-1-1 Katahira, Sendai, 980-8577, Japan.*
Electronic Supplementary Information (ESI) available: [details of any supplementary information available should be included here]. See DOI: 10.1039/x0xx00000x

The ***S*-1/*R*-1** reveals weak ferromagnetism realized from its spatial symmetry breaking, which Dzyaloshinskii–Moriya interactions could be activated. To the best of our knowledge, this is the first chiral weak ferromagnet found in a spin chain of deformed perovskite derivatives with corner-sharing octahedra structure of transition metal halide hydrates.

Experimental section

Materials synthesis

All reagents were commercially available and were used as received without further purification. First, 1 M HCl aqueous solution (2.3 mL) was added dropwise to a methanol solution (2 mL) of (*S*)- or (*R*)-*β*-methylphenethylamine (281.7 mg, 2.08 mmol). Then, $MnCl_2{\cdot}4H_2O$ (206.4 mg, 1.04 mmol) was added, and the solvents were boiled off. As a result, white powders of $[(S)\text{-MPA}]_2MnCl_4(H_2O)$ (***S*-1**) and $[(R)\text{-MPA}]_2MnCl_4(H_2O)$ (***R*-1**) were obtained as quantitative yield. (*S*)/(*R*)-MPA$^+$ is (*S*)/(*R*)-*β*-methylphenethylammonium ion. Elemental analysis (%) for ***S*-1** and ***R*-1** is as follows: For ***S*-1**: calculated for $C_{18}H_{30}Cl_4MnN_2O$: C, 44.38; H, 6.21; N, 5.75. Found: C, 44.49; H, 6.18; N, 5.88. For ***R*-1**: calculated for $C_{18}H_{30}Cl_4MnN_2O$: C, 44.38; H, 6.21; N, 5.75. Found: C, 44.55; H, 6.14; N, 5.74.

X-ray crystallographic analysis

Crystal data for ***S*-1/*R*-1** were collected at 103 K using a CCD diffractometer (Saturn 724 VariMax) with multilayer mirror monochromated Mo-Kα radiation (λ = 0.71073 Å). Single crystals with dimensions 0.182 × 0.046 × 0.032 mm^3 and 0.204 × 0.01 × 0.009 mm^3 for ***S*-1** and ***R*-1**, respectively, were mounted on thin Kapton films and cooled in an N_2 gas stream. The structures were solved using direct methods (SHELXL) and expanded using Fourier techniques. The nonhydrogen atoms were refined anisotropically, and the hydrogen atoms were refined using a rigid model. The detailed crystallographic data are shown in Tables S1 and S2. These data have been deposited as CIFs at the Cambridge Crystallographic Data Centre (CCDC) as publication no. CCDC-2190484 for ***S*-1** and CCDC- 2190483 for ***R*-1**.

Computational details

DFT calculations with a Gaussian basis set were performed for the organic cations, (*S*)-MPA$^+$ and (*R*)-MPA$^+$. The B3LYP/6-31G+(d) level of theory was used and all calculations were conducted using *Gaussian09*.

Magnetic properties measurements

Magnetic characteristics of ***S*-1/*R*-1** were observed using a Quantum Design MPMS magnetometer (MPMS-XL). The temperature dependence of magnetic susceptibility was measured with a magnetic field of 0.1 T for the polycrystalline sample, in the temperature range between 1.86 and 300 K. The remanent magnetization was measured in the warming process under 0 T after cooling the sample in 0.01 T. The magnetic field dependence of magnetization was recorded at 1.86 K by sweeping the magnetic field between −0.15 and 0.15 T. The temperature dependence of the alternating current (AC) magnetic susceptibility was observed with a 0.3 mT AC magnetic field in the frequency range between 1 and 1 kHz.

ESR spectra measurements

The ESR spectra were measured by utilizing a homemade transmission-type ESR system with a 15 T superconducting magnet at the High Field Laboratory for Superconducting Materials at Tohoku University. The ESR data were obtained from the measurements, using 81 Gunn oscillator (Millitech GDM-10-1019R) combined with a doubler (VDI WR4.3 × 2), and a Schottkey diode detector (ZBD WR-5.1).

Results and discussion

Needle-like colorless single crystals of ***S*-1/*R*-1** (Figure S1) were grown by evaporating a mixture of an HCl aqueous solution of $MnCl_2{\cdot}4H_2O$ and a methanol solution of (*S*)/(*R*)-*β*-methylphenethylamine. ***S*-1** and ***R*-1** crystalize in the monoclinic space group $P2_1$ involving both contents of chirality and polarity (Tables S1 and S2). The crystal structures of ***S*-1** and ***R*-1** form a mirror relationship between ***S*-1** and ***R*-1** (Figure 1a). In both of ***S*-1/*R*-1**, the 1D-chains of manganese chloride hydrates (i.e., $[MnCl_4(H_2O)]^{2-}$), consisting of corner sharing $MnCl_5(H_2O)$ octahedra, run along the *b* axis, which form a chain-aligned layer parallel to the *ab* plane (Figures. 1b and 1c). The $[MnCl_4(H_2O)]^{2-}$ chain layer is sandwiched by a double layer of (*S*)/(*R*)-MPA$^+$ (Figures 1a and 1b).

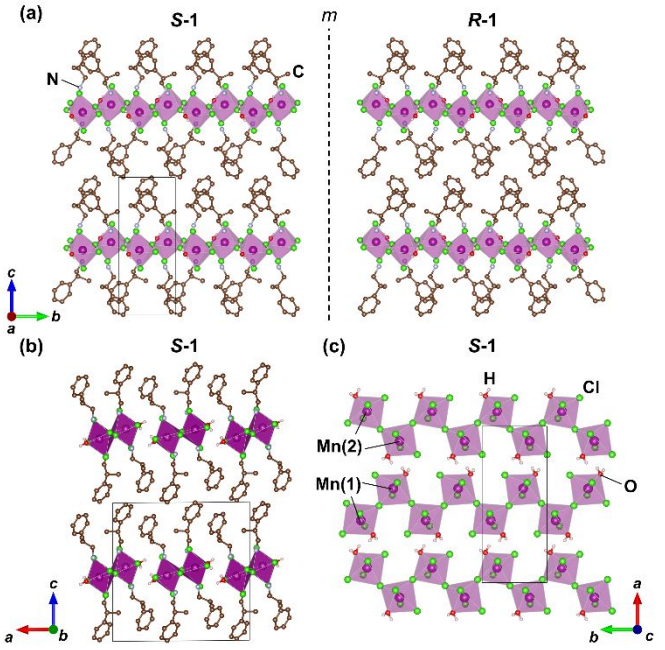

Figure 1. Crystal structures of (a) ***S*-1** and ***R*-1** projected along [100], (b) ***S*-1** projected along [010], and (c) ***S*-1** projected along [001] with color codes Mn (purple), Cl (yellowish green), C (brown), N (grey), O (red) and H (pale pink). Mn(1) and Mn(2) are crystallographically unique manganese sites in the unit cell. Hydrogen atoms are omitted for clarity except for those of H_2O. $MnCl_5(H_2O)$ units are displayed as polyhedral. *m* represents a mirror plane.

The asymmetric unit of ***S*-1/*R*-1** has four crystallographically unique (*S*)/(*R*)-MPA$^+$ cations. Each (*S*)/(*R*)-MPA$^+$ cation possesses an electric dipole moment (***p***), which originates from charge distributions in the ammonium and phenyl/alkyl groups in the (*S*)/(*R*)-MPA$^+$ cation, where the magnitude of ***p*** for the

(*S*)/(*R*)-MPA$^+$ cation was evaluated to be 12.3 D (averaged value) by density functional theory calculations (Figure S2). The ***p*** of (*S*)/(*R*)-MPA$^+$ cations cancel each other out along the *c* axis in the crystal packing (Figure S3), but the projected ***p*** on the *ab* plane are not cancelled, producing an electric polarization along the [010] direction (Figure S3).

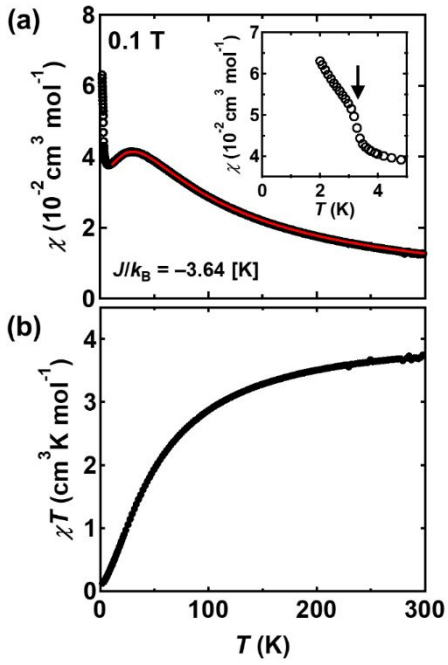

Figure 2. (a) Temperature dependence of magnetic susceptibility (χ) of ***S*-1** in 0.1 T. The inset magnifies the low temperature range of χ. The red line represents the curve fitted by modified Fisher's model. (b) Temperature dependences of χT for ***S*-1**.

Figures 2a and 2b show the temperature (T) dependence of the magnetic susceptibility (χ) and the χT product for ***S*-1** at an applied field (H) of 0.1 T measured in the temperature range of 2.0–300 K, respectively. With cooling, the χ gradually increases and passes through a maximum around 30 K. Upon further decreasing the temperature, the χ exhibits an upturn below 8 K. The χT value of ***S*-1**, which corresponds to 3.77 cm^3 K mol^{-1} at 300 K smaller than a spin-only value for S = 5/2 with g = 2.0, decreases continuously to 0.126 cm^3 K mol^{-1} at 2 K, indicating that an antiferromagnetic (AFM) interaction mainly through the bridging single Cl ion is dominant in ***S*-1** (Figure 2b). Here, taking account of the 1D chain form of $[MnCl_4(H_2O)]^{2-}$, the broad maximum near 30 K in the χ could be attributed to a typical linear chain of Heisenberg AFM behavior, representing the magnetic interaction along the individual chains of the Mn^{2+} (S = 5/2) ions. For such a uniform 1D chain of classical spins, the χ can be expressed by the modified Fisher's model[26] as

$$\chi = \frac{N_A g^2 \mu_B^2 S(S+1)}{3k_B T} \times \frac{1+u}{1-u} \qquad (1)$$

, where

$$u = \coth\left\{\frac{2JS(S+1)}{k_B T}\right\} - \frac{k_B T}{2JS(S+1)}$$

$$S = \frac{5}{2}$$

$$g = 2$$

The J represents the exchange parameter and is defined as negative for antiferromagnetic interactions: $H = -2J\sum S_i \cdot S_j$. As shown by the red curve in Figure 2a, the simulated curve with J/k_B = −3.64 K gave a good quantitative fit to the experimental data for ***S*-1** above 10 K by using the model.

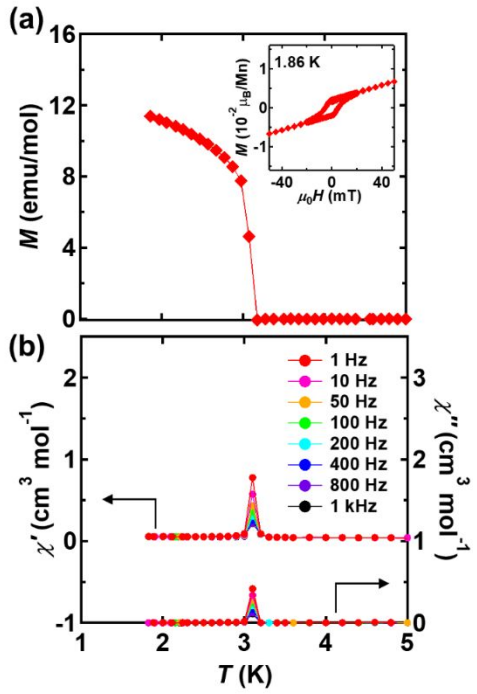

Figure 3. (a) Temperature dependence of the remanent magnetization of ***S*-1**. The inset shows magnetic field dependence of magnetization of ***S*-1** at 1.86 K. (b) Temperature dependence of AC susceptibility of ***S*-1**.

As for the rapidly increasing contribution of χ below 8 K, a shoulder-like anomaly was found around 3.2 K, implying the presence of long-range magnetic ordering. To clarify the origin of this anomaly, remanent magnetization (Figure 3a) and alternative current (AC) magnetic susceptibility (Figure 3b) were measured below 5 K. As a result, the spontaneous magnetization was observed below 3.2 K, at which the peak anomalies appear in both real- (χ') and imaginary- (χ'') parts of AC susceptibility. These results indicate that a long-range magnetic order with ferromagnetic (FM) component exist in this region. In fact, a hysteresis curve was confirmed in the magnetic field (H) dependence of the magnetization measured at 1.86 K as shown in the inset of Figure 3a. In the M–H curve, the saturation M of FM component is ca. 2.0×10^{-3} μ_B/Mn, which is much smaller than the full moment of Mn^{2+} (S = 5/2), 5 μ_B/Mn. The same magnetic characteristics were observed also in

enantiomer, ***R*-1** (Figures S4 and S5). Considering that the point group of ***S*-1/*R*-1** is noncentrosymmetric (C_2), the weak ferromagnetism could be ascribed to the canting of AFM spins induced by Dzyaloshinskii–Moriya interaction.

Figure 4a displays the absolute value of temperature (T) derivative of M, $|dM/dT|$, in the H ranging from 0 T to 7 T. Taking account that the peak in $|dM/dT|$ coincides with that of AC χ at 0 T, the phase boundary between a paramagnetic (PM) phase and a canted antiferromagnetic (CAFM) phase can be estimated from the $|dM/dT|$ peak in each H; the obtained magnetic phase diagram is depicted in Figure 4b. As the magnetic field increases, the CAFM transition temperature increases, indicating that the CAFM phase is stabilized by the Zeeman energy gain via a net magnetization.

The presence of CAFM phase was also confirmed by the electron spin resonance (ESR) spectroscopy. Figure 4c is ESR spectra of polycrystalline sample of ***S*-1** measured at a microwave of 162 GHz in the temperature range from 100 K to 4.2 K. In the ESR spectra above 10 K in the PM phase (Figure 4b), the single ESR absorption peak was observed at ca. 5.9 T, which is comparable with the resonant H for the transition of $\Delta m_S = \pm 1$, where m_S is a spin magnetic quantum number: $\mu_0 H = h\nu / g\mu_B \approx 5.8$ T with $g = 2$ and $\nu = 162$ GHz. In contrast, the peak splitting is observed at 4.2 K in the CAFM phase. In the case of Heisenberg linear chain magnets, it is known that the different ESR frequencies appear reflecting magnetic anisotropy when the H is applied along the chain and when it is applied perpendicularly.[44] In addition, it is also reported that the difference in frequencies increases with the development of spin correlations.[44] Thus, the observed splitting of ESR peak could be ascribed to the development of spin correlation in the CAFM phase.

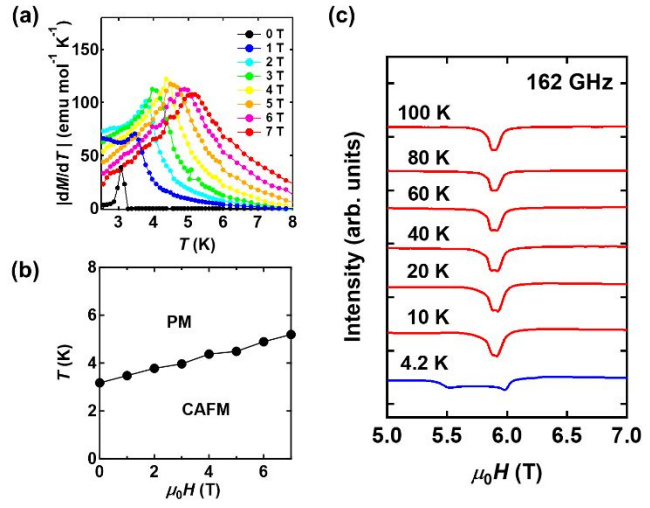

Figure 4. (a) Derivative of the magnetization (M) for ***S*-1** with respect to the temperature (T), dM/dT. The absolute values are displayed for each magnetic field. (b) Magnetic phase diagram of ***S*-1**. The phase boundary is estimated from the peak position of $|dM/dT|$ in Figure 4a. PM and CAFM represent paramagnetic and canted antiferromagnetic phases, respectively. (c) ESR spectra of polycrystal sample of ***S*-1**. The red and blue curves show the spectra in PM and CAFM, respectively.

Conclusions

In summary, we have developed a chiral 1D organic-inorganic manganese chloride hydrate $[(S)/(R)\text{-MPA}]_2[MnCl_4(H_2O)]$ and found a weak ferromagnetic phase as the ground state. So far, the compound in this work is the only chiral 1D Mn^{II} chain with a singly bridged mode showing weak ferromagnetism. The lack of such materials may be resolved by applying synthesis under high pressure, high temperature, or other unique methods. Since both spatial inversion symmetry and time reversal symmetry are broken in this type of materials, the novel magneto-electric coupling phenomena would be expected to emerge from this platform in the further study.

Conflicts of interest

There are no conflicts to declare.

Acknowledgements

This work was supported by PRESTO JST (JPMJPR19L4). This work was partly supported by a Grants-in-Aid for Scientific Research (Grant Nos. 21H01026, 20H01829, 20H00381, 18K19050, 18H05208) from JSPS, and the E-IMR project. P.-J. H. is thankful for the JSPS Research Fellowship for Young Scientists (No. 18J20896).

Notes and references

1 G. L. J. A. Rikken and E. Raupach, *Nature* 1997, **390**, 493–494.
2 C. Train, R. Gheorghe, V. Krstic, L.-M. Chamoreau, N. S. Ovanesyan, G. L. J. A. Rikken, M. Gruselle and M. Verdaguer, *Nat. Mater.* 2008, **7**, 729–734.
3 Y. Kitagawa, H. Segawa and K. Ishii, *Angew. Chem. Int. Ed.* 2011, **50**, 9133–9136.
4 M. Ceolín, S. Coberna-Ferrón and J. R. Galán-Mascarós, *Adv. Mater.* 2012, **24**, 3120–3123.
5 R. Sessoli, M.-E. Boulon, A. Caneschi, M. Mannini, L. Poggini, F. Wilhelm and A. Rogalev, *Nat. Phys.* 2015, **11**, 69–74.
6 K. Taniguchi, M. Nishio, S. Kishiue, P.-J. Huang, S. Kimura and H. Miyasaka, *Phys. Rev. Mat.* 2019, **3**, 045202.
7 K. Taniguchi, S. Kishiue, S.Kimura and H. Miyasaka, *J. Phys. Soc. Jpn.* 2019, **88**, 093708.
8 G. L. J. A. Rikken, J. Fölling and P. Wyder, *Phys. Rev. Lett.* 2001, **87**, 236602.
9 F. Pop, P. Auban-Senzier, E. Canadell, G. L. J. A. Rikken and N. Avarari, *Nat. Commun.* 2014, **5**, 3757.
10 T. Yokouchi, N. Kanazawa, A. Kikkawa, D. Morikawa, K. Shibata, T. Arima, Y. Taguchi, F. Kagawa and Y. Tokura, *Nat. Commun.* 2017, **8**, 866.
11 F. Qin, W. Shi, T. Ideue, M. Yoshida, A. Zak, R. Tenne, T. Kikitsu, D. Inoue, D. Hashizume and Y. Iwasa, *Nat. Commun.* 2017, **8**, 14465.
12 S. Mühlbauer, B. Binz, F. Jonietz, C. Pfleiderer, A. Rosch, A. Neubauer, R. Georgii and P. Böni, *Science* 2009, **323**, 915–919.
13 X. Z. Yu, Y. Onose, N. Kanazawa, J. H. Park, J. H. Han, Y. Matsui, N. Nagaosa and Y. Tokura, *Nature* 2010, **465**, 901–904.
14 S. Seki, X. Z. Yu, S. Ishiwata and Y. Tokura, *Science* 2012, **336**, 198–201.
15 K. Taniguchi, M. Nishio, N. Abe, P.-J. Huang, S. Kimura, T.

Arima and H. Miyasaka, *Angew. Chem. Int. Ed.* 2021, **60**, 14350–14354.
16 D. G. Billing and A. Lemmerer, *CrystEngComm* 2006, **8**, 686–695.
17 C.-K. Yang, W.-N. Chen, Y.-T. Ding, J. Wang, Y. Rao, W.-Q. Liao, Y.-Y. Tang, P.-F. Li, Z.-X. Wang, R.-G. Xiong, *Adv. Mater.* 2019, **31**, 1808088.
18 P.-J. Huang, K. Taniguchi and H. Miyasaka, *J. Am. Chem. Soc.* 2019, **141**, 14520–14523.
19 P.-J. Huang, K. Taniguchi, M. Shigefuji, T. Kobayashi, M. Matsubara, T. Sasagawa, H. Sato and H. Miyasaka, *Adv. Mater.* 2021, **33**, 2008611.
20 P.-J. Huang, K. Taniguchi and H. Miyasaka, *Chem. Mater.* 2022, **34**, 4428−4436.
21 B. Sun, X.-F. Liu, X.-Y. Li, Y. Zhang, X. Shao, D. Yang and H.-L. Zhang, *Chem. Mater.* 2020, **32**, 8914–8920.
22 C. Yuan, X. Li, S. Semin, Y. Feng, T. Rasing and J. Xu, *Nano Lett.* 2018, **18**, 5411–5417.
23 C. Chen, L. Gao, W. Gao, C. Ge, X. Du, Z. Li, Y. Yang, G. Niu and J. Tang, *Nat. Commun.* 2019, **10**, 1927.
24 A. Ishii and T. Miyasaka, *Sci. Adv.* 2020, **6**, eabd3274.
25 Y. Hu, F. Florio, Z. Chen, W. A. Phelan, M. A. Siegler, Z. Zhou, Y. Guo, R. Hawks, J. Jiang, J. Feng, L. Zhang, B. Wang, Y. Wang, D. Gall, E. F. Palermo, Z. Lu, X. Sun, T.-M. Lu, H. Zhou, Y. Ren, E. Wertz, R. Sundararaman and J. Shi, *Sci. Adv.* 2020, **6**, eaay4213.
26 R. Dingle, M. E. Lines, and S. L. Holt, *Phys. Rev.* 1969, **187**, 643−648.
27 Q. Guo, W.-Y. Zhang, C. Chen, Q. Ye, and D.-W. Fu, *J. Mater. Chem. C* 2017, **5**, 5458−5464.
28 Y. M. You, W.-Q. Liao, D. Zhao, H.-Y. Ye, Y. Zhang, Q. Zhou, X. Niu, J. Wang, P.-F. Li, D.-W. Fu, Z. Wang, S. Gao, K. Yang, J.-M. Liu, J. Li, Y. Yan, and R.-G. Xiong, *Science* 2017, **357**, 306–309.
29 H.-Y. Ye, Q. Zhou, X. Niu, W.-Q. Liao, D.-W. Fu, Y. Zhang, Y. M. You, J. Wang, Z.-N. Chen, and R.-G. Xiong, *J. Am. Chem. Soc.* 2015, **137**, 13148–13154.
30 Y. Zhang, W.-Q. Liao, D.-W. Fu, H.-Y. Ye, C.-M. Liu, Z.-N. Chen, and R.-G. Xiong, *Adv. Mater.* 2015, **27**, 3942–3946.
31 S. J. Jensen, *Acta Chem. Scand.* 1967, **21**, 889−898.
32 R. E. Caputo, and R. D. Willett, *Acta Cryst.* 1981, **B37**, 1618−1619.
33 W. Depmeier, *Acta Cryst.* 1980, **B36**, 1065−1068.
34 T. Maris, and R. Zouari, *Acta Cryst.* 2003, **E59**, m1201−m1203.
35 D. J. Carnevale, L. N. Dawe, C. P. Landee, M. M. Turnbull, and J. L. Wikaira, *Polyhedron* 2021, **202**, 115200.
36 J.-H. P. Lee, B. D. Lewis, J. M. Mendes, M. M. Turnbull, and F. F. Awwadi, *J. Coord. Chem.* 2003, **56**, 1425−1442.
37 C. Han, D. B. Cordes, A. M. Z. Slawin, and P. Lightfoot, *Crystals* 2020, **10**, 930.
38 T. Naito, and T. Inabe, *J. Solid State Chem.* 2003, **176**, 243−249.
39 L. V. Zorina, T. G. Prokhorova, S. S. Khasanov, S. V. Simonov, V. N. Zverev, A. V. Korobenko, A. V. Putrya, V. S. Mironov, E. Canadell, R. P. Shibaeva, and E. B. Yagubskii, *CrystEngComm* 2009, **11**, 2102−2109.
40 J.-X. Gao, W.-Y. Zhang, Z.-G. Wu, Y.-X. Zheng, and D.-W. Fu, *J. Am. Chem. Soc.* 2020, **142**, 4756−4761.
41 H.-L. Xuan, Y.-F. Sang, L.-J. Xu, D.-S. Zheng, C.-M. Shi, and Z.-N. Chen, *Chem. Eur. J.* 2022, **28**, e202201299.
42 J. Cirera, Y. Jiang, L. Qin, Y.-Z. Zheng, G. Li, G. Wu, and E. Ruiz, *Inorg. Chem. Front.* 2016, **3**, 1272−1279.
43 M. R. Silva, A. M. Beja, J. A. Paixão and J. Martín-Gil, *J. Solid State Chem.* 2006, **179**, 2054−2058.
44 K. Nagata and Y. Tazuke, *J. Phys. Soc. Jpn.* 1972, **32**, 337–345.